

Cold-Cap Temperature Profile Comparison between the Laboratory and Mathematical Model – 15591

Derek R Dixon ^{*}, Michael J Schweiger ^{*}, Brian J Riley ^{*}, Richard Pokorny ^{**}, and Pavel Hrma ^{*}

^{*}Pacific Northwest National Laboratory, Richland, WA 99354, derek.dixon@pnnl.gov

^{**}Department of Chemical Engineering, Institute of Chemical Technology Prague, Technicka 5, 166 28 Prague 6, Czech Republic

ABSTRACT

The rate of waste vitrification in an electric melter is connected to the feed-to-glass conversion process, which occurs in the cold cap, a layer of reacting feed on top of molten glass. The cold cap consists of two layers: a low-temperature (~100°C – ~800°C) region of unconnected, reacting feed and a high-temperature (~800°C – ~1100°C) region of molten glass with gas bubbles and cavities. A recently developed mathematical model describes the effect of the cold cap on glass production. For verification of the mathematical model, a cold cap produced in a laboratory-scale melter was subsequently analyzed by correlating structural features of a polished region with those obtained in heat-treated feed samples to determine the temperature profile as a function of cold-cap position. After corrections were made for the diminished volume of bubbles and collapsed cavities that occurred in the cold-cap sample during cooling, the temperature gradients were alike in the model and the laboratory cold cap through the range from ~500°C to ~1100°C. The temperature profiles were different in the upper region of the cold cap because the radiant heat from the molten glass in the laboratory-scale melter resulted in dry and hot (~400°C) surface conditions whereas the model assumed a surface covered by boiling slurry.

INTRODUCTION

Background

In an electric melter, like those being constructed for the Hanford Tank Waste Treatment and Immobilization Plant (WTP) [1, 2], the waste vitrification rate is related to the conversion of the melter slurry feed into molten glass [3-5]. This conversion occurs in a layer of reacting feed floating on top of molten glass called the cold cap [3-5]. A schematic representation of the cold cap is shown in Fig. 1. The cold cap is comprised of two layers: the reacting feed layer from ~100°C to ~800°C and the foam layer (including the primary foam, cavities, and secondary foam shown in Fig. 1) from ~800°C to ~1100°C [5]. The gas bubbles in the primary foam are generated from the evolved CO₂ and NO_x in the glass-forming reactions, while those in the secondary foam result from O₂ production in the redox reactions in molten glass [3, 5]. The foam layer significantly reduces the heat transfer from the molten glass to the reacting feed and, as a result, limits the melt rate [5].

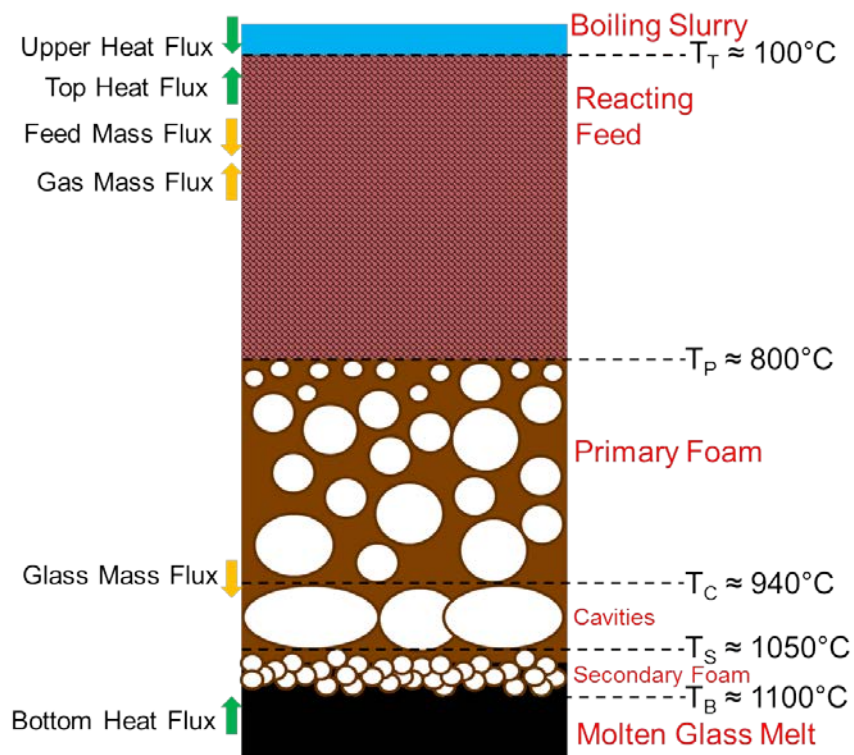


Fig. 1. Schematic of the structure and temperature profile in a cold cap (adapted from Pokorny and Hrma [5]). Here, T_T is the top surface temperature, T_P is the primary foam temperature, T_C is the cavity temperature, T_S is the secondary foam temperature, and T_B is the bottom glass temperature.

Mathematical models of electric glass-melting furnaces can serve to increase the melting rate by simulating a variety of different glass compositions and conditions. However, the models reported in the literature did not account for the effect of the cold cap [6-8]; some models include the reacting feed layer, but without considering the insulating properties of foam [9, 10]. A recently developed mathematical model by Pokorny and Hrma [4, 5, 11] estimates the melting rate of the glass by representing the temperature field in both the reacting feed and the foam layer as realistically as possible.

For verification of this mathematical model, the experimental determination of the temperature distribution within a laboratory-made cold cap is therefore essential. In this study, a laboratory-scale melter (LSM), which enabled the preservation of the cold cap, was used to study the internal microstructure of the cold cap via sectioning and analysis [12-14]. The temperature distribution within the cold cap was determined by comparing scanning electron micrographs located at different areas within the cold cap with those from feed samples heated to set temperatures. The temperature distribution was also verified through comparison of the fractions of the major crystalline components at those same areas by x-ray diffraction [14].

The continued improvement of this mathematical model by comparison with the temperature profile in a laboratory-created cold cap is crucial to understanding the characteristics of the cold cap and their effect on the glass production rate in an electric melter. In its current iteration, the model is designed to simulate the vitrification of the high-level waste (HLW) fraction at the Hanford WTP [5]. The HLW is set to contain the majority of the short-lived activity radionuclides like cesium-137 and strontium-90, the volatilities of which are inhibited by the presence of the cold cap covering 90-100% of the glass surface in a melter [15]. The mathematical model has the ability to predict crucial characteristics of the cold cap that

may be important to restricting radionuclide volatility and ultimately shorten the life cycle of waste cleanup at the Hanford site by predicting the glass production rates of hundreds of different feeds [16].

Feed Composition

A simulated HLW feed called A0 (Table I) was used for this study [3-5, 12-14]. The glass produced from the A0 feed has a high Al₂O₃ content (~24%) [16]. For the LSM cold cap, a feed amount that would produce 400 g of glass was added to ~800 mL of deionized water to create a slurry of 400 g glass per liter [14].

Table I. A0 Feed Composition for 400 g of Glass

Compound	Amount (g)
Al(OH) ₃	146.99
B(OH) ₃	107.93
Bi(OH) ₃	5.12
CaO	24.31
Fe(H ₂ PO ₂) ₃	4.97
Fe(OH) ₃	29.53
KNO ₃	1.22
Li ₂ CO ₃	35.32
Mg(OH) ₂	0.68
Na ₂ C ₂ O ₄	0.50
Na ₂ CrO ₄	4.46
Na ₂ SO ₄	1.42
NaF	5.91
NaNO ₂	1.35
NaOH	39.77
NiCO ₃	2.54
Pb(NO ₃) ₂	2.43
SiO ₂	122.02
Zn(NO ₃) ₂ ·4H ₂ O	1.06
Zr(OH) ₄ ·0.65H ₂ O	2.19
Total	539.74

Mathematical Model Development

Four simulation parameters were varied in the calculation of the mathematical model to determine their effects on the cold cap characteristics: T_B ; the height of the cavity layer (h_C); the fraction of the heat supplied to the cold cap by the plenum (f_{plenum}); and the foaminess constant (Φ). The foaminess constant is a measure of the response extent in the connected, secondary foam layer glass as gas flows from the melt below, as defined by Equation (1):

$$\Phi = \frac{h_S}{j_{sg}} \quad (1)$$

where h_s is the height of the secondary foam layer and j_{sg} is the volumetric gas phase flux entering the secondary foam from the melt [5, 17].

The baseline values applied for these parameters were $T_B = 1100^\circ\text{C}$, $h_C = 7$ mm, $f_{\text{plenum}} = 0.5$, and $\Phi = 400$ s. To calculate all values in the foam layer for each solution of the model, an iterative approach was required. Using this approach, initial values were given for T_C , T_S , and the melting rate, from which the cold-cap thickness and time-temperature history were calculated leading to the average heating rate for the feed in the cold cap. From this average heating-rate value, new values for the heat transferred through the foam layer, T_C , and T_S were calculated leading to a new value for the melting rate. Iteration of this calculation continued until a steady-state melting rate was achieved as determined by a small difference between the amount of heat transferred through the foam layer and the heat necessary for melting [5].

The height of the secondary foam layer is shown to increase with respect to foaminess where $h_S < 1$ mm at $\Phi = 100$ s, $h_S \approx 1$ mm at $\Phi = 400$ s, and $h_S \approx 3$ mm at $\Phi = 1000$ s [5]. Fig. 2 shows the effect of T_B and foaminess on the cold-cap thickness, T_C , and melting rate [5]. As T_B increases, T_C and the melting rate increase, while the cold-cap thickness decreases. As foaminess increases, T_C and the melting rate decrease, while the cold-cap thickness increases. In addition, the temperature distribution as a function of position in the cold cap, with $\Phi = 400$ s, is shown in Fig. 3 for a $T_B = 1050^\circ\text{C}$ and $T_B = 1100^\circ\text{C}$ [5].

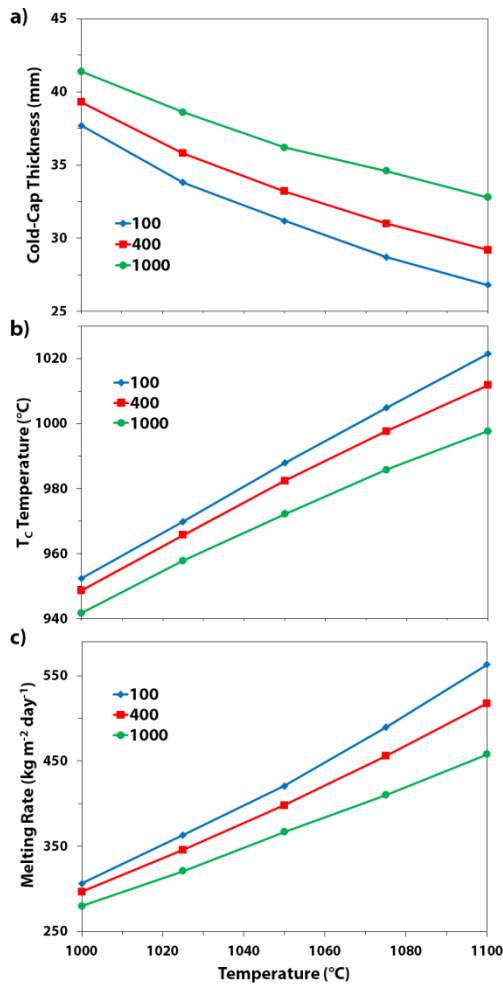


Fig. 2. The a) cold-cap thickness, b) cavity temperature (T_C), and c) melting rate generated from the mathematical model at varying levels of foaminess (Φ).

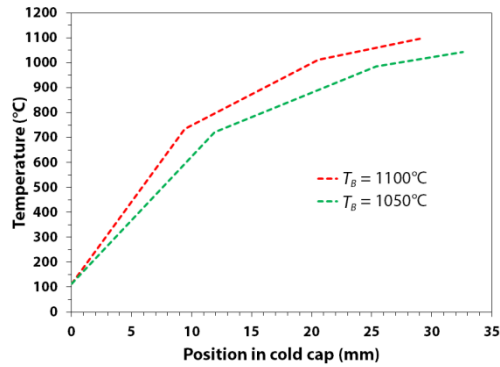


Fig. 3. Temperature profile in the cold cap given two different T_B values, 1050 and 1100°C.

LSM Cold Cap Characteristics

The cold cap produced in the LSM, which was compared to the mathematical model in this study, is shown in Fig. 4 [14]. The LSM was run with the temperature of the glass melt greater than that of the mathematical model, where $T_B = 1200^\circ\text{C}$. The extent of exposed glass melt surface in the LSM crucible allowed dry feed to accumulate at $\sim 400^\circ\text{C}$ on top of the cold cap [4, 9, 14]. As a result, $f_{\text{plenum}} > 0.5$ in the LSM cold cap. Since the glass melt in the LSM used previously-melted glass fragments, very few O_2 bubbles were generated from redox reactions below the cold cap [14], i.e., foaminess was very low, $\Phi \approx 100$ s. Feed was charged into the LSM for 35 min and steady state was not achieved under these conditions [14]. The primary foam was not able to coalesce to form large cavities causing $h_C \approx 0$ mm.

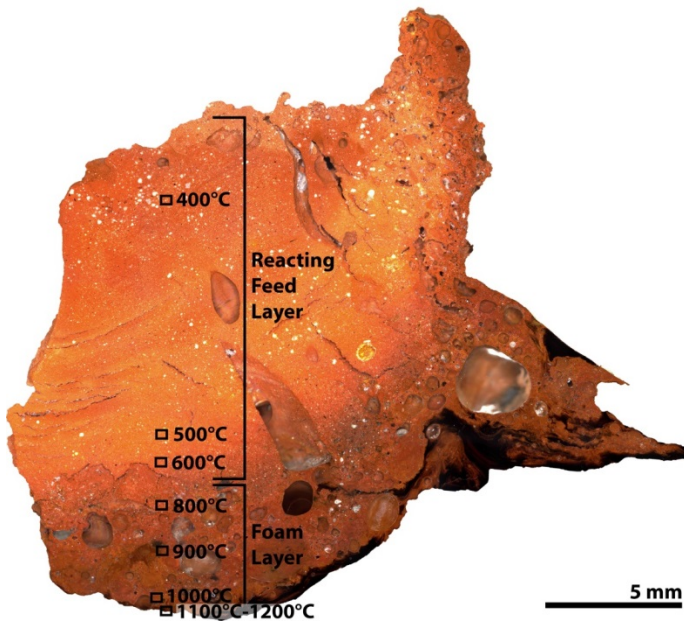


Fig. 4. Temperature profile of the laboratory-made cold cap.

EXPERIMENTAL

Mathematical-Model Temperature Profile Adaptation

Wet-feed conditions, where the melter head space heat flux (Q_U) is less than that of the heat necessary to evaporate the slurry (Q_{UC}), were used in the calculation of the mathematical-model temperature profile, causing the heat for slurry evaporation to transfer through the cold cap while $T_T \approx 100^\circ\text{C}$ [5]. Attempts to replicate the dry-feed condition ($Q_U > Q_{UC}$) in the mathematical model by increasing $T_T \approx 300^\circ\text{C}$ resulted in a divergence in the calculations [14].

Since the dry-feed cold-cap condition could not be achieved in the mathematical model, only the portion of the mathematical-model temperature profile unaffected by the low-temperature feed accumulation, from 500°C to T_B , was used for comparison with the LSM cold-cap temperature profile. As such, the 0 mm (top) position in the temperature profile was set to 500°C .

LSM Cold-Cap Temperature Profile Adaptation

First, the 500°C area was set to the 0 mm (top) position in the LSM cold-cap temperature profile as detailed above. Additionally, the rapid quenching method employed to preserve the LSM cold-cap upon the end of feed charging caused gas bubbles in the foam layer to shrink to ~ 0.5 their original size, based on the ideal gas law, as they cooled from $\sim 1000^\circ\text{C}$ to $\sim 500^\circ\text{C}$. Considering the average porosity (p) of the foam layer to be 0.5 [18], the average size of the foam layer would be expected to be $\sim 1.5\times$ larger during the run than after quenching [14]. To account for the bubble size shrinkage upon cooling, the foam layer ($\sim 800^\circ\text{C} - \sim 1200^\circ\text{C}$) of the LSM cold-cap temperature profile was corrected by a factor of 1.5.

RESULTS AND DISCUSSION

Temperature Profile Comparison

The cold-cap temperature profiles, as calculated by mathematical model and determined from the LSM, are compared in Fig. 5a. Three intervals are observed in the temperature profiles. The first interval, from 500°C to $\sim 800^\circ\text{C}$ corresponds to the reacting feed layer of the cold cap with open porosity. The steep temperature gradient in this interval is a result of the low effective heat conductivity of the feed [5]. The mathematical models and LSM cold cap exhibit nearly identical temperature gradients in this interval. The second interval, from $\sim 800^\circ\text{C}$ to $\sim 1000^\circ\text{C}$, matches with the primary foam layer. In this interval, the LSM cold-cap has a higher temperature-gradient than that in the mathematical model. This difference resulted from the bubble shrinkage correction factor applied in the case of the LSM cold cap, which can be increased to account for additional factors, such as gas bubbles that may have escaped from under the cold cap upon quenching. The third interval spans the temperature region from $\sim 1000^\circ\text{C}$ to the T_B of each profile. A stark difference between the mathematical-models and the LSM cold-cap profiles is observed in this interval, which pertains to the lack of cavities and secondary foam in the case of the LSM cold cap. These layers ($h_C + h_S$) have a total thickness of ~ 8 mm in the mathematical model.

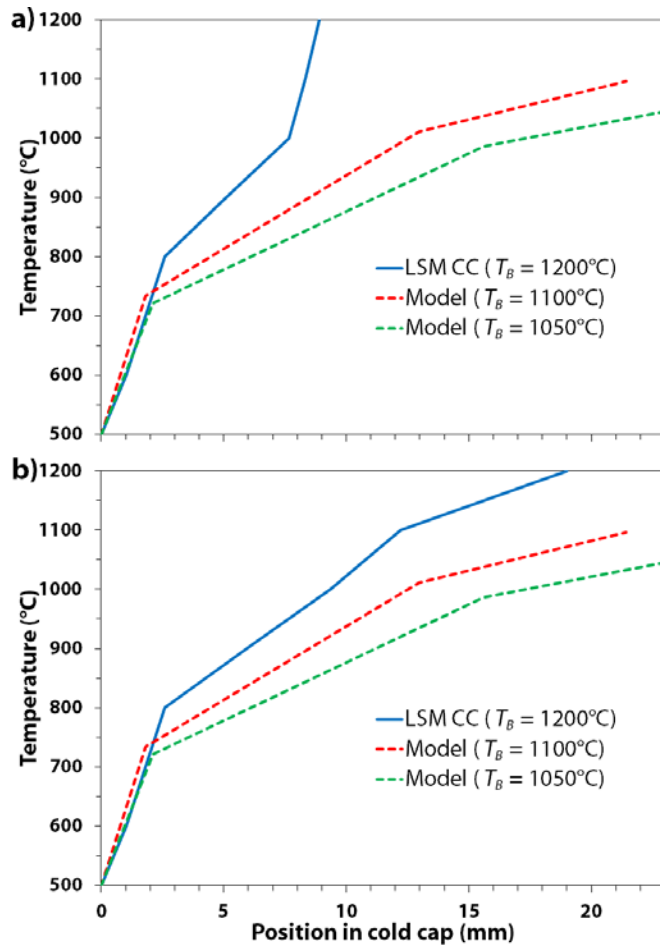


Fig. 5. Comparison of the temperature profiles in the laboratory-scale melter cold cap (LSM CC) at 1200°C and those calculated in the mathematical model cold cap at 1050 and 1100°C a) with a bubble shrinkage correction factor of 1.5 and b) with a correction factor of 2 while also accounting for $(h_C + h_S) = 8$ mm.

The LSM cold-cap temperature profile using a correction factor of 2 and adding the 8 mm into the secondary foam temperature region is shown in Fig. 5b. The trend of cold-cap properties as T_B increases in the mathematical model indicates that the total cold-cap thickness will decrease at $T_B = 1200^\circ\text{C}$ as was used in the LSM cold cap. This adjustment further account for the differences in all three of the intervals of the temperature profiles.

CONCLUSIONS

The temperature profile of a cold cap produced in a laboratory-scale melter was compared with one calculated from a mathematical model. Radiant heating in the laboratory-scale melter resulted in a large accumulation of dry feed at $\sim 400^\circ\text{C}$, which could not be replicated in the mathematical model, so the resultant temperature profiles were analyzed from 500°C to the temperature of the molten glass melt. The resulting profiles compared favorably in the open porosity layer from 500°C to $\sim 800^\circ\text{C}$. After applying a correction factor to the temperature profile to account for the shrinkage of gas bubbles upon cooling in the laboratory-scale melter cold-cap, the gradients were similar in the primary foam layer from $\sim 800^\circ\text{C}$ to $\sim 1000^\circ\text{C}$. The cavity and secondary foam layers were not present in the laboratory-scale melter for comparing the region from $\sim 1000^\circ\text{C}$ to the glass melt. Future iterations of the mathematical model will

WM2015 Conference, March 15 – 19, 2015, Phoenix, Arizona USA

work to reconcile the differences between the temperature profiles by changing the temperature of the glass melt, the size of the cavity layer, and foaminess.

REFERENCES

1. BECHTEL NATIONAL INC, "About The Project," <http://www.hanfordvitplant.com/page/the-project/> (2013).
2. P.J. CERTA, P.A. EMPEY, M.N. WELLS, "River Protection Project System Plan," ORP-11242 Rev. 6, U.S. Department of Energy Office of River Protection, Richland, Washington (2011).
3. D.A. PIERCE, P. HRMA, J. MARCIAL, B.J. RILEY, M.J. SCHWEIGER, "Effect of Alumina Source on the Rate of Melting Demonstrated with Nuclear Waste Glass Batch," *International Journal of Applied Glass Science*, **3**, 59-68 (2012).
4. R. POKORNY, P. HRMA, "Mathematical modeling of cold cap," *Journal of Nuclear Materials*, **429**, 245-256 (2012).
5. R. POKORNY, P. HRMA, "Model for the conversion of nuclear waste melter feed to glass," *Journal of Nuclear Materials*, **445**, 190-199 (2014).
6. Z. FENG, D. LI, G. QIN, S. LIU, "Study of the Float Glass Melting Process: Combining Fluid Dynamics Simulation and Glass Homogeneity Inspection," *Journal of the American Ceramic Society*, **91**, 3229-3234 (2008).
7. C.C. YEN, W.S. HWANG, "Numerical Study of Fluid Flow Behaviors in an Alkali-Free Glass Melting Furnace," *Materials Transactions*, **49**, 766-773 (2008).
8. A. ABBASSI, K. KHOSHMANESH, "Numerical simulation and experimental analysis of an industrial glass melting furnace," *Applied Thermal Engineering*, **28**, 450-459 (2008).
9. P. HRMA, "Thermodynamics of batch melting," *Glastechnische Berichte-Glass Science and Technology*, **55**, 138-150 (1982).
10. P. SCHILL, J. CHMELAR, "Use of computer flow dynamics in glass technology," *Journal of Non-Crystalline Solids*, **345-346**, 771-776 (2004).
11. P. HRMA, A.A. KRUGER, R. POKORNY, "Nuclear waste vitrification efficiency: Cold cap reactions," *Journal of Non-Crystalline Solids*, **358**, 3559-3562 (2012).
12. D.R. DIXON, M.J. SCHWEIGER, P. HRMA, "Effect of Feeding Rate on the Cold Cap Configuration in a Laboratory-Scale Melter," *WM2013 Conference*, Paper#13362, Phoenix, AZ (2013).
13. D.R. DIXON, M.J. SCHWEIGER, P. HRMA, "Characterizing a High-Level Waste Cold Cap via Elemental and Structural Configuration," *WM2014 Conference*, Paper#14185, Phoenix, AZ (2014).
14. D.R. DIXON, M.J. SCHWEIGER, B.J. RILEY, R. POKORNY, P. HRMA, "Temperature Distribution within a High-Level Waste Cold Cap," In Preparation (2015).
15. J.S. MCCLOY, B.J. RILEY, A. GOEL, M. LIEZERS, M.J. SCHWEIGER, C.P. RODRIGUEZ, P. HRMA, D.-S. KIM, W.W. LUKENS, A.A. KRUGER, "Rhenium Solubility in Borosilicate Nuclear Waste Glass: Implications for the Processing and Immobilization of Technetium-99," *Environmental Science & Technology*, **46**, 12616-12622 (2012).
16. J. MARCIAL, J. CHUN, P. HRMA, M. SCHWEIGER, "Effect of Bubbles and Silica Dissolution on Melter Feed Rheology during Conversion to Glass," *Environmental Science & Technology*, **48**, 12173-12180 (2014).
17. J.J. BIKERMAN, "The unit of foaminess," *Transactions of the Faraday Society*, **34**, 634-638 (1938).
18. P. HRMA, M. SCHWEIGER, C. HUMRICKHOUSE, J. MOODY, R. TATE, T. RAINSDON, N. TEGROTENHUIS, B. ARRIGONI, J. MARCIAL, C. RODRIGUEZ, B. TINCHER, "Effect of Glass-Batch Makeup on the Melting Process," *Ceramics-Silikaty*, **54**, 193-211 (2010).

ACKNOWLEDGMENTS

This work was supported by the U.S. Department of Energy's Waste Treatment and Immobilization Plant Federal Project Office under the direction of Dr. Albert A. Kruger. The Pacific Northwest National

WM2015 Conference, March 15 – 19, 2015, Phoenix, Arizona USA

Laboratory is operated for the Department of Energy by Battelle Memorial Institute under contract DE AC05 76RL0 1830. A portion of the research was performed at the Environmental Molecular Sciences Laboratory (EMSL), a DOE Office of Science user facility sponsored by the Office of Biological and Environmental Research and located at Pacific Northwest National Laboratory. The authors would like to thank Shelley Carlson for mounting and polishing all specimens for SEM work and Dong-Sang Kim for his help in discussions about this research.